Erythromelalgia caused by the missense mutation p.Arg220Pro in an alternatively spliced exon of SCN9A (Na$_V$1.7)

Jennifer R. Deuis[1],[†], Smitha Kumble[2],[3],[†], Angelo Keramidas[1], Lotten Ragnarsson[1], Cas Simons[2], Lynn Pais[4], Susan M. White[3],[5],[*],

Irina Vetter[1],[6],[*]

[1]Institute for Molecular Bioscience, 306 Carmody Road, The University of Queensland, St Lucia, QLD 4072, Australia
[2]Murdoch Children's Research Institute, 50 Flemington Road, Royal Children's Hospital, Parkville, VIC 3052, Australia
[3]Department of Paediatrics, The University of Melbourne, 50 Flemington Road, Parkville, VIC 3052, Australia
[4]Program in Medical and Population Genetics, Broad Institute of MIT and Harvard, 415 Main Street, Cambridge, MA 02142, United States
[5]Victorian Clinical Genetics Services, Royal Children's Hospital, 50 Flemington Road, Parkville, VIC 3052, Australia
[6]School of Pharmacy, 20 Cornwall Street, The University of Queensland, Woolloongabba, QLD 4102, Australia

*Corresponding authors. Institute for Molecular Bioscience, The University of Queensland, St Lucia, QLD, Australia. E-mail: i.vetter@uq.edu.au; Victorian Clinical Genetics Services, Royal Children's Hospital, Parkville, VIC, Australia. E-mail: sue.white@vcgs.org.au
[†]Jennifer R. Deuis and Smitha Kumble contributed equally.

Abstract

Erythromelalgia (EM), is a familial pain syndrome characterized by episodic 'burning' pain, warmth, and erythema. EM is caused by monoallelic variants in *SCN9A*, which encodes the voltage-gated sodium channel (Na$_V$) Na$_V$1.7. Over 25 different *SCN9A* mutations attributed to EM have been described to date, all identified in the *SCN9A* transcript utilizing exon 6N. Here we report a novel *SCN9A* missense variant identified in seven related individuals with stereotypic episodes of bilateral lower limb pain presenting in childhood. The variant, XM_011511617.3:c.659G>C;p.(Arg220Pro), resides in the exon 6A of *SCN9A*, an exon previously shown to be selectively incorporated by developmentally regulated alternative splicing. The mutation is located in the voltage-sensing S4 segment of domain I, which is important for regulating channel activation. Functional analysis showed the p.Arg220Pro mutation altered voltage-dependent activation and delayed channel inactivation, consistent with a Na$_V$1.7 gain-of-function molecular phenotype. These results demonstrate that alternatively spliced isoforms of *SCN9A* should be included in all genomic testing of EM.

Keywords: erythromelalgia; Na$_V$1.7; pain; electrophysiology

Introduction

Erythromelalgia (EM) is a rare familial pain syndrome characterized by episodic 'burning' pain, warmth, and erythema (redness), most commonly affecting the extremities [1]. The distribution of symptoms can progress proximally over time to include the limbs and face. The painful episodes are usually bilateral, are often triggered by heat or exercise, and can be relieved by exposure of the affected limbs to cold temperatures. EM is caused by pathogenic monoallelic variants in *SCN9A*, which encodes the voltage-gated sodium channel Na$_V$1.7. Na$_V$1.7 is one of nine human Na$_V$ channels that is highly expressed on nociceptive or "pain-sensing" neurons, where it contributes to action potential generation at peripheral nerve terminals and neurotransmitter release at central terminals [2, 3]. Over 25 different *SCN9A* mutations attributed to EM have been described to date, with varying effects on Na$_V$1.7 function (due to the mutations being diffusely spread), resulting overall in a gain-of-function at the channel level [4].

Na$_V$ channels are formed by four homologous domains (DI–DIV), with each domain consisting of six α-helical transmembrane segments termed S1–S6 [5]. Segments S1–S4 assemble to form the voltage-sensing domain (VSD) whereas segments S5–S6 assemble to form the Na$^+$ selective pore module [6]. Each

S4 segment contains four to eight positively charged residues (arginine or lysine), each separated by two hydrophobic residues. These charged residues form the gating charges, which move outward in response to membrane depolarization to cause voltage-dependent channel opening [7].

Duplication of a gene encoding an ancestral two-domain channel is believed to have led to the splicing of Na$_V$ channels [8, 9]. The mutually exclusive versions of exon 6, referred to as 6A (adult) or 6N (neonatal), encode the S3–S4 extracellular linker and the S4 voltage sensor of the first domain. The splicing at exon 6 is conserved in six mammalian sodium channel genes (*SCN1A*, *SCN2A*, *SCN3A*, *SCN5A*, *SCN8A* and *SCN9A*) and generally changes one amino acid in DI S3–S4 from asparagine or serine to a negatively charged aspartic acid [10]. The expression of exon 6 splice variants is developmentally regulated, has subtle effects on Na$_V$ channel biophysics, and allows for functional diversity from a single gene [11, 12]. Despite the nomenclature, *SCN9A* isoforms containing both the 6A and 6N exons are expressed at roughly equal levels in adult rodent dorsal root ganglion (DRG) neurons [13]. While most biophysical parameters between the two *SCN9A* isoforms are the similar, *SCN9A* transcripts containing exon 6A generate larger ramp currents [14].

While the developmentally regulated alternative splicing of *SCN9A* has been extensively characterized, these biophysically

relevant splicing events are not well represented in the mRNA catalogs typically used to identify disease-causing variants as part of clinical genomic testing. The representative transcript for *SCN9A* selected as part of the MANE project by NCBI and EMBL-EBI is NM_001365536.1, and it utilizes exon 6N. This transcript contains all reported Pathogenic and Likely Pathogenic variants recorded in ClinVar to date. The Refseq database does not contain any curated transcripts (denoted by the NM_ prefix) that contain exon 6A: it can only be found in the computationally predicted transcripts such as XM_011511617.3.

Here, we report a *SCN9A* variant, XM_011511617.3:c.659G>C; p.Arg220Pro, identified in seven related individuals with stereotypic episodes of bilateral lower limb pain presenting in childhood. This variant resides in exon 6A of *SCN9A* and, to our knowledge, is the first disease-associated *SCN9A* variant that is not present in the exon 6N *SCN9A* transcript [15, 16].

Results

Clinical presentation and molecular genetics identify the novel Na$_V$1.7 mutation p.Arg220Pro

The clinical presentation of episodic distal pain in multiple family members raised suspicion for an inherited neuropathic pain disorder. The phenotype in the family presents as an atypical form of EM, as erythema, swelling and redness were not present in four individuals and not a prominent symptom for any family member. The distribution of pain in several family members was particularly in the popliteal fossae and ankles, which is atypical for EM.

Genomic sequencing identified a novel heterozygous variant in *SCN9A*, hg38:chr2:g.166304060C>G that was present in both affected individuals sequenced. The variant lies deep within intron 6 of the SCN9A transcript utilizing exon 6N (NM_001365536.1:c.688 + 178G>C) making it unlikely to alter the final protein product. However, in the alternative transcripts that utilize exon 6A, the variant results in a arginine to proline substitution XM_011511617.3:c.659G>C; p.Arg220Pro (Fig. 1B).

The residue p.Arg220 is highly conserved residue across vertebrates and is also conserved across the Na$_V$ channels subtypes (Na$_V$1.1–Na$_V$1.8) (Fig. 2). The variant is absent from control populations (gnomAD v3.1.2 and v2.1) and *in silico* tools predict the variant to be damaging. Subsequent Sanger sequencing determined that the variant was present in all seven affected family members.

The mutation p.Arg220Pro alters the biophysical properties of Na$_V$1.7 consistent with a gain-of-function phenotype

To assess the effect of p.Arg220Pro substitution on the function of Na$_V$1.7, we transiently expressed WT Na$_V$1.7 and Na$_V$1.7-p.Arg220Pro in HEK293 cells and compared currents using whole-cell patch-clamp electrophysiology (Fig. 3A). The p.Arg220Pro mutation had no effect on the V$_{50}$ of the voltage-dependence of activation (V$_{50}$ WT -28.2 ± 1.0 mV; V$_{50}$ p.Arg220Pro -26.5 ± 1.4 mV; unpaired *t*-test, $P = 0.3491$). However, an increase in the slope factor (*k*) of the conductance–voltage curve was observed (WT 2.6 ± 0.3; p.Arg220Pro 7.7 ± 0.5; unpaired *t*-test, $P < 0.0001$) (Fig. 3B and C). An increase in the slope factor indicates that the p.Arg220Pro mutant has a higher conductance at more hyperpolarizing membrane potentials, causing early channel opening compared to WT, consistent with gain-of-function. The p.Arg220Pro mutation also significantly altered the activation and inactivation kinetics of Na$_V$1.7, causing a voltage-dependent

increase in the time to peak (Fig. 3D) and a prominent voltage-dependent delay in fast inactivation (Fig. 3E). The p.Arg220Pro mutation also shifted the voltage-dependence of steady-state fast inactivation (V$_{50}$ WT -70.5 ± 0.7 mV; V$_{50}$ p.Arg220Pro -65.7 ± 1.3 mV; unpaired *t*-test, $P = 0.0064$) (Fig. 3F) and reduced the proportion of channels available for activation at the time intervals indicated, without changing the time constant τ_1 of recovery from fast inactivation (τ_1 WT 4.59 ± 0.5 ms; τ_1 p.Arg220Pro 6.06 ± 0.5 ms; unpaired *t*-test, $P = 0.0697$) (Fig. 3G).

The mutation p.Arg220Pro has no effect on Na$_V$1.7 ramp currents

In peripheral sensory neurons, Na$_V$1.7 is the primary voltage-gated sodium channel responsible for ramp currents, which are currents that occur in response to slow depolarizing stimuli [17]. Ramp currents are thought to be important for amplifying small depolarizations and bringing the membrane potential to threshold to fire an action potential [18].

In response to a depolarizing ramp of 1 mV/ms (Fig. 4A), the peak ramp current size (WT -77 ± 9 pA; p.Arg220Pro -99 ± 8 pA; unpaired *t*-test, $P = 0.1126$; Fig. 4B) and the time to peak (WT 70 ± 6 ms; p.Arg220Pro 63 ± 1 ms; unpaired *t*-test, $P = 0.2611$; Fig. 4C) were not different between WT Na$_V$1.7 and Na$_V$1.7-p.Arg220Pro, indicating the mutation had minimal effect on ramp currents.

Carbamazepine has minimal effect on the gating of Na$_V$1.7-p.Arg220Pro

The anti-epileptic drug, carbamazepine (CBZ) is a non-selective Na$_V$ inhibitor often trialed in the management of EM symptoms that can correct the hyperpolarized voltage-dependence of activation in some Na$_V$1.7 EM mutants *in vitro* [19–21]. We therefore assessed the effect of carbamazepine on the functional properties of Na$_V$1.7-p.Arg220Pro channel. At a concentration of 500 μM, which far exceeds clinically achievable plasma concentrations, CBZ inhibited Na$_V$1.7-p.Arg220Pro peak current (Fig. 5A) but was unable to correct the increased slope (*k*) of the conductance-voltage curve (buffer 7.6 ± 1; CBZ 8.9 ± 0.9; paired *t*-test, $P = 0.0775$; Fig. 5B). While CBZ was able to enhance the rate of fast inactivation (Fig. 5C), the rate was not returned to that of WT Na$_V$1.7.

Discussion

Here, we describe a novel *SCN9A* variant that causes EM. To our knowledge, this is the first report of a disease-causing *SCN9A* variant located in the alternatively spliced exon 6A. The designation of one splice variant as 'canonical' and one as 'alternative' in public databases has led to the misinterpretation of other *SCNxA* variants. For example, a pathogenic *SCN1A* variant that leads to decreased expression of Na$_V$1.1 in the brain was initially mistaken for an intronic variant, but then later shown to reside in the 'alternative' exon 20N [22, 23]. In addition, pathogenic mutations for *SCN8A* and *SCN9A* that reside in the coding region of exon 6 have been described, but the splice variant 6A or 6N is often not specified [15, 24].

The clinical presentation of this family is most in keeping with an atypical EM due to the stereotypical distribution of pain. EM typically involves the extremities, most commonly affecting the feet and hands [25]. Pain can progress proximally with disease progression to involve the lower legs and arms and infrequently, the face and ears [25]. Pain confined to only the lower limbs is not uncommon [26]. However, the pattern of popliteal fossa and ankle pain with sparing of the distal extremities reported in the
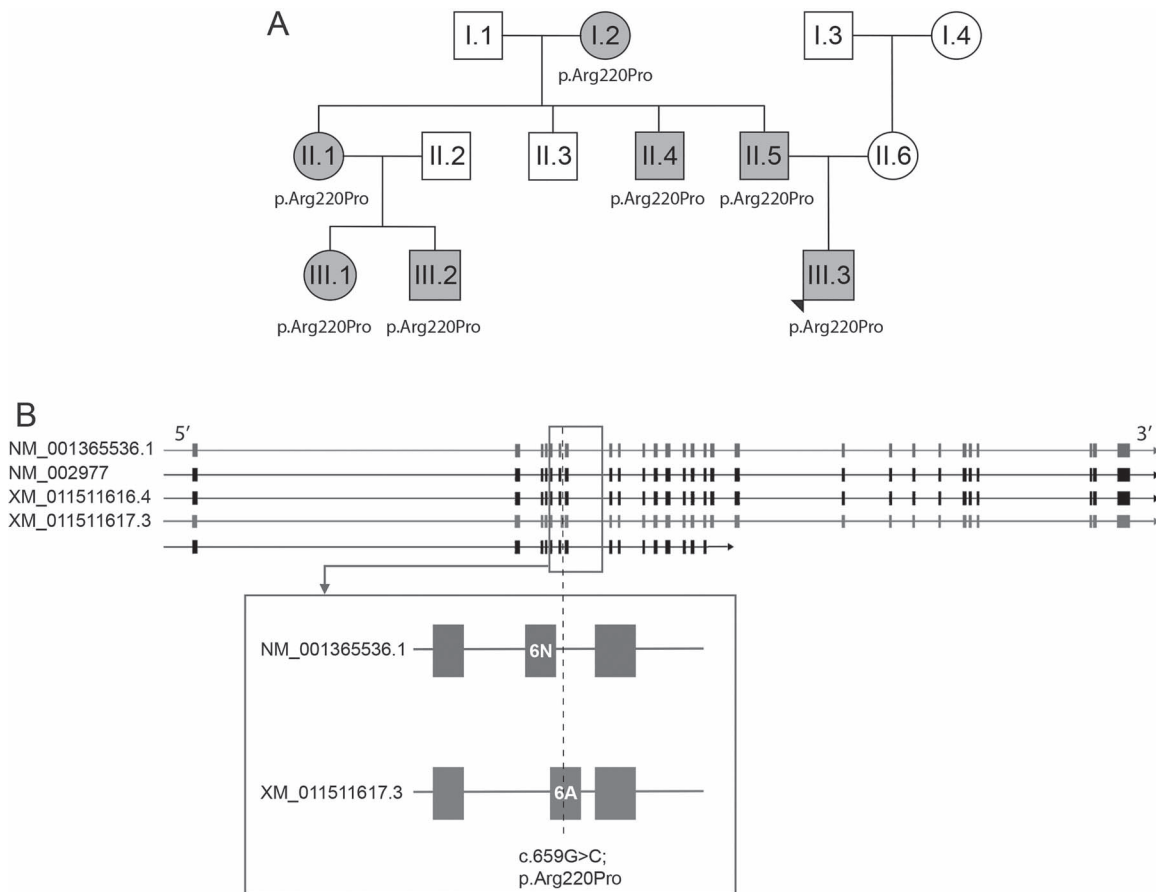
Figure 1. (A) Family pedigree showing clinically affected individuals (shaded) and those with confirmed p.Arg220Pro variants. (B) Diagram of the *SCN9A* gene and associated transcripts showing the position of the p.Arg220Pro variant. In the transcript NM_001365536.1, the variant is in intron 6. In the alternative transcript XM_011511617.3 the variant lies within exon 6A.
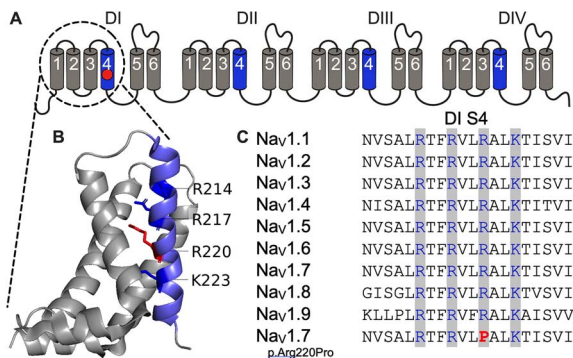

Figure 2. The p.Arg220Pro Na$_V$1.7 variant is located on the R3 gating charge of the S4 transmembrane segment on DI. (A) Linear representation of Na$_V$1.7 illustrating the assembly of the transmembrane segments into four domains (DI–DIV), each consisting of six transmembrane segments (S1–S6). The location of the p.Arg220Pro mutation is indicated by the red circle. (B) Cryo-electron microscopy structure of the voltage-sensing domain formed by the S1–S4 transmembrane segments of DI (PDB 6J8I). The S4 transmembrane segment containing the four gating charges is colored blue. p.Arg220Pro is the third gating charge (R3). (C) Sequence alignment of DI S4 transmembrane segment of human Na$_V$1.1-Na$_V$1.8. The four conserved positively charged amino acids residues are colored blue.

members and was not reported to be a prominent feature. All family members in this study had a striking lean build: this is not a known reported association with *SCN9A* mutations and may represent a separate trait segregating in the family.

The cause of the atypical clinical presentation in this family is not clear. It may be explained by phenotypic variability, which has previously been reported both within and between families with this condition [26, 28]. While greater hyperpolarizing shifts in Na$_V$1.7 channels are reported to correlate with early symptom onset and slower progression [26], there have been no correlations with anatomical pain distribution or associated symptoms.

The localization of the variant in exon 6A may also contribute to the atypical clinical presentation in this family. This disease-causing variant will be co-expressed with wild-type transcripts that encode the mutually exclusive exon 6N. Furthermore, the ratio of affected to unaffected transcripts will reflect the developmental and tissue-specific expression of the gene, as the variant will only be present in a subset of *SCN9A* transcripts [8]. While the Na$_V$1.7-p.Arg220Pro variant leads to multiple "gain-of-function" changes at the channel level, it remains to be confirmed what impact this has on excitability at the neuronal level. Given that mutant Na$_V$1.7 channels are co-expressed with wildtype Na$_V$1.7 channels, it is likely the overall impact on neuronal excitability will be more nuanced, and may explain the atypical presentation of EM.

Our data shows that the Nav1.7-p.Arg220Pro variant affects multiple functional properties of the channels, which is consistent with the important function of the gating charges

proband, has not previously been reported in patients with EM [26, 27]. Associated erythema, warmth and swelling is a consistently reported feature [26, 27] but only present in three of the family
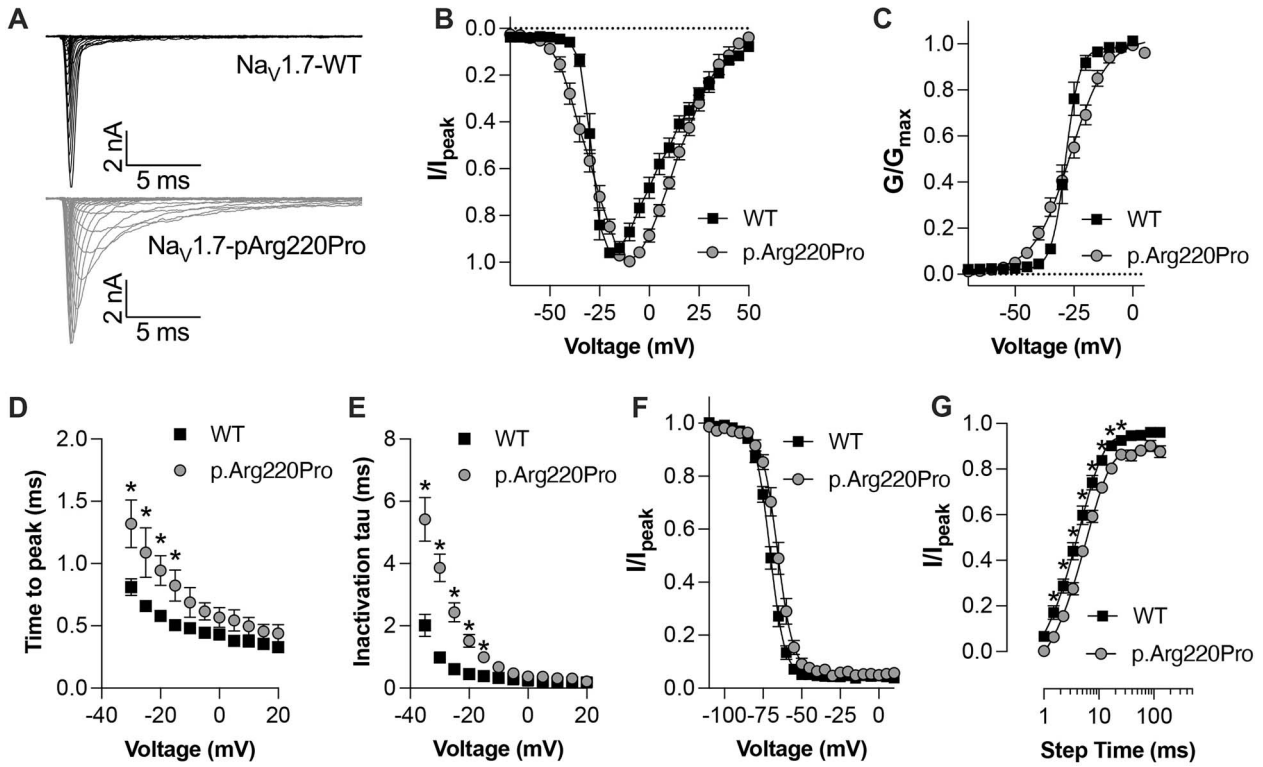
Figure 3. Biophysical characterization of Na$_V$1.7-p.Arg220Pro mutant. (A) Representative current traces recorded from HEK293 cells expressing Na$_V$1.7 WT and Na$_V$1.7-p.Arg220Pro. (B) Current–voltage (I-V) relationship of Na$_V$1.7 WT (n = 8) and Na$_V$1.7-p.Arg220Pro (n = 5). Data represents peak inward current connected by a continuous line. (C) Conductance-voltage (G-V) relationship of Na$_V$1.7 WT (n = 8) and Na$_V$1.7-p.Arg220Pro (n = 5). Data is fitted to a Boltzmann equation. (D) Time to peak calculated from pulse onset to peak inward current of Na$_V$1.7 WT (n = 8) and Na$_V$1.7-p.Arg220Pro (n = 5). (E) Fast inactivation time constants as determined by a single exponential fit of Na$_V$1.7 WT (n = 8) and Na$_V$1.7-p.Arg220Pro (n = 5) currents. (F) Voltage-dependence of steady-state fast inactivation of Na$_V$1.7 WT (n = 7) and Na$_V$1.7-p.Arg220Pro (n = 5). Data is fitted to a Boltzmann equation. (G) Recovery from fast inactivation fitted to a single-exponential function of Na$_V$1.7 WT (n = 5) and Na$_V$1.7-p.Arg220Pro (n = 4). Data are presented as mean ± SEM. Statistical significance for panels D, E and G was determined using two-way ANOVA, $*P < 0.05$.
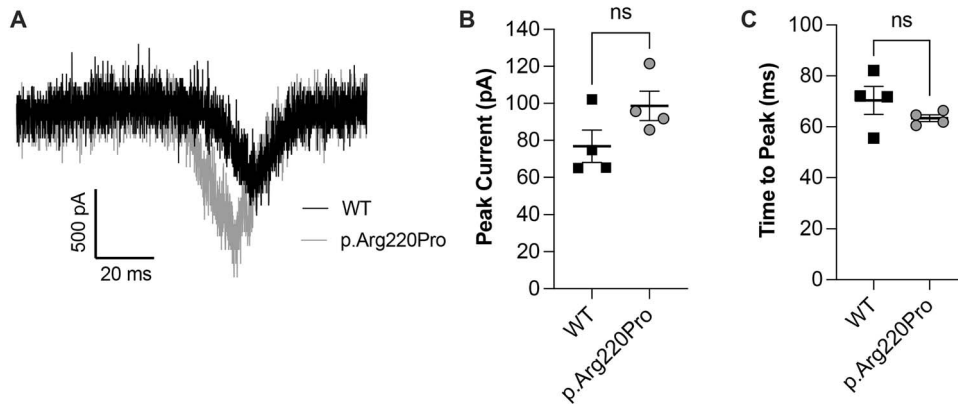

Figure 4. Effect of the p.Arg220Pro mutation on Na$_V$1.7 ramp currents. (A) Representative ramp current trace of Na$_V$1.7 WT overlayed with Na$_V$1.7-p.Arg220Pro. Currents were elicited from −100 mV to +20 mV using a slow depolarizing ramp of 1 mV/ms. (B) Peak current and (C) time to peak of Na$_V$1.7 WT and Na$_V$1.7-p.Arg220Pro taken from the ramp protocol described above. Data are presented as mean ± SEM (n = 4). Statistical significance was determined using unpaired t-test, $*P < 0.05$.

on the S4 transmembrane segments for regulating voltage-dependent channel opening and closing. While most EM mutations cause a hyperpolarizing shift in the voltage-dependence of activation [4], the p.Arg220Pro mutation had no effect on the V$_{50}$ of activation. Instead, it caused a shallower slope in the conductance-voltage curve, resulting in channels that open earlier and closer to resting membrane potential. This early channel opening in combination with the profound delay in fast inactivation likely both contribute to the EM channelopathy.

This inference is based on toxins that activate Na$_V$ channels by causing early channel opening, such as β-scorpion toxins and ciguatoxin, or by delaying/disrupting fast inactivation, such as α-scorpion toxins and δ-theraphotoxins, both being able to enhance neuronal excitability and cause profound spontaneous nociceptive behaviors in rodents [29–32].

This study is the first to report a channelopathy associated with the p.Arg220Pro mutation on Na$_V$1.7 channels. The equivalent mutation, p.Arg225Pro on the Na$_V$1.5 cardiac subtype,
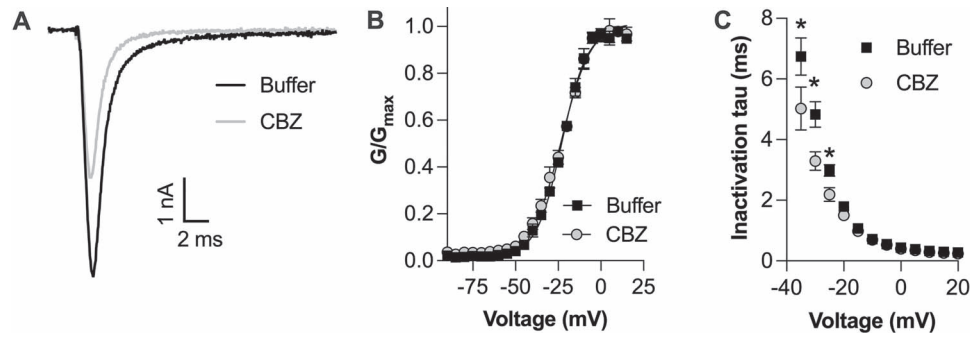
Figure 5. Effect of carbamazepine on the biophysics of Na$_V$1.7-p.Arg220Pro. (A) Representative current trace of Na$_V$1.7-p.Arg220Pro before and after addition of 500 μM carbamazepine (CBZ). Currents were elicited by a 50 ms pulse to -20 mV from a holding potential of -90 mV. (B) Conductance-voltage relationship of Na$_V$1.7-p.Arg220Pro before and after addition of 500 μM carbamazepine. Data is fitted to a Boltzmann equation. (C) Fast inactivation time constants as determined by a single exponential fit of Na$_V$1.7-p.Arg220Pro currents before and after addition of 500 μM carbamazepine. Data are presented as mean $\pm$ SEM (n = 4). Statistical significance for panel C was determined using two-way ANOVA, $*P < 0.05$.

has previously been reported in a patient with multifocal ventricular ectopy-associated cardiomyopathy [33]. The effects of p.Arg225Pro on Na$_V$1.5 function are similar to those reported on Na$_V$1.7 here, causing an increase in the slope of the conductance-voltage curve without altering the V$_{50}$ of activation, and a delay in the kinetics of fast inactivation.

Conclusion

In summary, we have described a novel missense mutation in exon 6A of SCN9A that results in atypical EM. Functional studies demonstrate that mutation of the R3 gating charge from an arginine to a proline on domain I disrupts the normal functional properties of the Na$_V$1.7 channel, causing a reduction in current decay kinetics, a shallowing in the slope of the conductance-voltage curve, and a delay in the time to peak. Our results confirm the importance of the domain I R3 gating charge for regulating Na$_V$1.7 voltage-dependence of activation, which if perturbed by mutation, gives rise to neuropathic pain.

Materials and Methods
Subjects

Research activities were carried out under institutional ethics approval HREC36291A. The proband and all affected family members have provided consent to be included in this publication. Detailed clinical phenotyping of the proband was performed by a neurologist and clinical geneticist. Additional clinical details were provided by affected family members.

The proband, Individual III.3 (Fig. 1A), is one of two sons to unrelated parents. He was born at 34 weeks' gestation via cesarean section due to placenta previa. He had an admission to neonatal intensive care due to poor respiratory effort and feeding difficulties.

From age five years he experienced episodes of pain in both popliteal fossae, and both ankles. Precipitants include strenuous exercise and intercurrent illness such as viral infections. The pain mostly occurred at night and was improved by plunging his lower limbs into cold water or applying ice. Movement also improved symptoms and some relief was experienced with non-steroidal anti-inflammatory medication and amitriptyline. There was no change in color or swelling of the lower limbs. There was no pain of his feet, hands, or face. He was otherwise healthy, and his learning, vision and hearing were all reported to be normal.

At last assessment at age 11.75 years, he had a lean build with height on the 19th centile and weight on the 0.1st centile. He had an unusual, crouched gait. He had prominent joints and there was some increased joint laxity at the ankle joints bilaterally. Beighton score was zero.

Nerve conduction studies, single nucleotide polymorphism (SNP) microarray and brain and spine MRI were all normal.

Several family members are also similarly affected (Fig. 1A), with symptom onset reported between ages 7–12 years. On specific questioning, three affected individuals reported occasional flushing of the skin of the extremities associated with their symptoms and two individuals report involvement of the feet and occasionally the hands. Affected family members reported that their symptoms improved over time. All affected individuals have a similar lean build.

Genomic sequencing

Whole Exome Sequencing (WES) on DNA extracted from blood samples from Individuals III.2 and III.3 was performed by the Broad Institute Center for Mendelian Genomics. Genomic data analysis using seqr was performed by clinicians and scientists at the Victorian Clinical Genetics Services [34]. Genomic variant pathogenicity was established according to the American College of Medical Genetics and Genomics/Association for Molecular Pathology (ACMG/AMP) criteria [35]. To determine if the variant was segregating with clinical features, Sanger sequencing of all affected family members was performed by the Murdoch Children's Research Institute.

Cell culture

Human Embryonic Kidney (HEK) 293 cells stably expressing the human Na$_V$ beta subunits β1/β2 (SB Drug Discovery, Glasgow, UK) were cultured in Minimum Essential Medium (MEM) supplemented with 10% fetal bovine serum (FBS) and 2 mM L-glutamine. Cells were grown in an incubator at 37°C with 5% CO$_2$ and passaged every 3–4 days (at 90% confluency).

Na$_V$1.7 mutagenesis

Wild-type (WT) human Na$_V$1.7 (hNav1.7) cDNA in the exon 6A/12S splice variant (NM_002977, a gift from Dr James Cox, University College London) was subjected to *in vitro* site-directed mutagenesis using the QuikChange™ XL mutagenesis kit (Agilent Technologies) following the manufacturer's instructions. Firstly, two amino acid mutations were introduced in the S3 membrane-spanning segment of domain I, exon 5, to convert the exon 6N

splice variant (200 Y**L**TEFV**N**LGNVS) to the exon 6A variant (200 Y**V**TEFV**D**LGNVS) of the hNa$_V$1.7 channel using the following two oligonucleotides: 5′-GCGTATGTAACAGAATTTGTAGACCTAGGCA ATG-3′ and 5′-CATTGCCTAGGTCTACAAATTCTGTTACATACGC-3′. The mutations were verified by sequencing through the Australian Genome Research Facility. The p.Arg220Pro point mutation was created in the hNa$_V$1.7 6A splice variant cDNA using the following two oligonucleotides: 5′-CGAACTTTCAGAGTATTGCCAGC TTTGAAAACTATTTC-3′ and 5′-GAAATAGTTTTCAAAGCTGGCAA TACTCTGAAAGTTCG-3′. The mutation was verified by sequencing through the Australian Genome Research Facility.

Transfection

Na$_V$1.7 and Na$_V$1.7-p.Arg220Pro were transiently transfected into HEK293 cells stably expressing β1/β2 using Lipofectamine 2000 (Thermo Fisher Scientific) according to manufacturer's instructions. After 24 h at 37°C, the medium containing transfection reagents was replaced, and cells were moved to 28°C with 5% CO$_2$ for another 24 h prior to patch-clamp experiments to increase surface expression of Na$_V$1.7.

Automated patch-clamp experiments

Automated whole-cell patch-clamp recordings were performed with a QPatch-16 automated electrophysiology platform (Sophion Bioscience, Ballerup, Denmark) using single-hole (QPlate 16 with a standard resistance of 2 ± 0.4 MΩ). Whole-cell currents were filtered at 8 kHz and acquired at 25 kHz and the linear leak was corrected by P/4 subtraction (leak potential −90 mV, leak sweep amplitude 10%). Series resistance across recorded cells ranged between 5–10 MΩ and was compensated at 70%.

The extracellular solution (ECS) consisted of (in mM) 70 NaCl, 70 choline chloride, 4 KCl, 2 CaCl$_2$, 1 MgCl$_2$, 10 HEPES, and 10 glucose, pH to 7.4 with NaOH (adjusted to 305 mOsm/L with sucrose). The intracellular solution (ICS) consisted of (in mM) 140 CsF, 1 EGTA, 5 CsOH, 10 HEPES, and 10 NaCl, pH to 7.3 with CsOH (adjusted to 320 mOsm/L with sucrose).

I-V curves were obtained with a holding potential of −90 mV followed by a series of 50 ms step pulses that ranged from −110 to +80 mV in 5-mV increments (repetition interval 6 s). For Na$_V$1.7-p.Arg220Pro the I-V protocol was performed before and after 5 min incubation of 500 μM carbamazepine (Sigma-Aldrich, Castle Hill, NSW, Australia).

Conductance-voltage (*G-V*) plots for peak current were obtained by calculating the conductance (*G*) at each voltage (*V*) using the equation $G = I/(V - V_{rev})$, where V_{rev} is the reversal potential. *G-V* curves were fitted with a Boltzmann equation. From this equation the V_{50}, defined as the membrane voltage at which 50% of channels are open, was computed.

The voltage dependence of steady-state fast inactivation was examined using a 10 ms pulse of −20 mV immediately after a series of 500 ms step pulses that ranged from −110 to +80 mV in 5 mV increments (repetition interval 6 s) to assess the available non-inactivated channels. The peak current at each test pulse was normalized and fitted using a Boltzmann equation.

The time constant of fast inactivation (τ) was computed by fitting the current decay traces with a single exponential function using QPatch Assay Software 5.6 (Sophion). The time to peak was calculated from pulse onset to peak inward current using QPatch Assay Software 5.6 (Sophion).

Recovery from fast inactivation was assessed using a two-pulse voltage protocol with a variable duration between pulses. To determine the proportion of recovered channels, the current from the second pulse (0 mV for 50 ms) was normalized to the current

from the first pulse (0 mV for 20 ms), and the duration between the pulses (holding potential −90 mV) was increased with each sweep by a factor of 1.5, from 1 ms to 129.7 ms, with a sweep interval of 20 s. Normalized currents were plotted versus pulse duration and fitted with a single exponential function.

Ramp currents were elicited using a slow depolarizing ramp from −100 mV to +20 mV at a rate of 1 mV/ms (120 ms duration). Time to peak was calculated from ramp onset to peak inward current using QPatch Assay Software 5.6 (Sophion).

Data analysis

Data were plotted and analyzed using GraphPad Prism version 9.0.0. Statistical significance was defined as $P < 0.05$ using tests as indicated. Data are presented as mean $\pm$ SEM.

Data availability

The data that support the findings of this study are available on request from the corresponding authors.

References

1. Tang Z, Chen Z, Tang B. *et al.* Primary erythromelalgia: a review. *Orphanet J Rare Dis* 2015;**10**:127.
2. Alexandrou AJ, Brown AR, Chapman ML. *et al.* Subtype-selective small molecule inhibitors reveal a fundamental role for Nav1.7 in nociceptor electrogenesis, axonal conduction and presynaptic release. *PLoS One* 2016;**11**:e0152405.
3. Minett MS, Nassar MA, Clark AK. *et al.* Distinct Nav1.7-dependent pain sensations require different sets of sensory and sympathetic neurons. *Nat Commun* 2012;**3**:791.
4. Vetter I, Deuis JR, Mueller A. *et al.* NaV1.7 as a pain target—from gene to pharmacology. *Pharmacol Ther* 2017;**172**:73–100.
5. Catterall WA, Goldin AL, Waxman SG. International Union of Pharmacology. XLVII. Nomenclature and structure-function relationships of voltage-gated sodium channels. *Pharmacol Rev* 2005;**57**:397–409.

6. Ahern CA, Payandeh J, Bosmans F. *et al.* The hitchhiker's guide to the voltage-gated sodium channel galaxy. *J Gen Physiol* 2016;**147**: 1–24.

7. Catterall WA, Wisedchaisri G, Zheng N. The chemical basis for electrical signaling. *Nat Chem Biol* 2017;**13**:455–63.

8. Raymond CK, Castle J, Garrett-Engele P. *et al.* Expression of alternatively spliced sodium channel alpha-subunit genes. Unique splicing patterns are observed in dorsal root ganglia. *J Biol Chem* 2004;**279**:46234–41.

9. Plummer NW, McBurney MW, Meisler MH. Alternative splicing of the sodium channel SCN8A predicts a truncated two-domain protein in fetal brain and non-neuronal cells. *J Biol Chem* 1997;**272**:24008–15.

10. Copley RR. Evolutionary convergence of alternative splicing in ion channels. *Trends Genet* 2004;**20**:171–6.

11. Liavas A, Lignani G, Schorge S. Conservation of alternative splicing in sodium channels reveals evolutionary focus on release from inactivation and structural insights into gating. *J Physiol* 2017;**595**:5671–85.

12. Gazina EV, Richards KL, Mokhtar MB. *et al.* Differential expression of exon 5 splice variants of sodium channel α subunit mRNAs in the developing mouse brain. *Neuroscience* 2010;**166**: 195–200.

13. Choi JS, Cheng X, Foster E. *et al.* Alternative splicing may contribute to time-dependent manifestation of inherited erythromelalgia. *Brain* 2010;**133**:1823–35.

14. Chatelier A, Dahllund L, Eriksson A. *et al.* Biophysical properties of human Na v1.7 splice variants and their regulation by protein kinase A. *J Neurophysiol* 2008;**99**:2241–50.

15. Estacion M, Choi JS, Eastman EM. *et al.* Can robots patch-clamp as well as humans? Characterization of a novel sodium channel mutation. *J Physiol* 2010;**588**:1915–27.

16. Drenth JP, te Morsche RH, Guillet G. *et al.* SCN9A mutations define primary erythermalgia as a neuropathic disorder of voltage gated sodium channels. *J Invest Dermatol* 2005;**124**: 1333–8.

17. Cummins TR, Howe JR, Waxman SG. Slow closed-state inactivation: a novel mechanism underlying ramp currents in cells expressing the hNE/PN1 sodium channel. *J Neurosci* 1998;**18**: 9607–19.

18. Rush AM, Cummins TR, Waxman SG. Multiple sodium channels and their roles in electrogenesis within dorsal root ganglion neurons. *J Physiol* 2007;**579**:1–14.

19. Fischer TZ, Gilmore ES, Estacion M. *et al.* A novel Nav1.7 mutation producing carbamazepine-responsive erythromelalgia. *Ann Neurol* 2009;**65**:733–41.

20. Yang Y, Dib-Hajj SD, Zhang J. *et al.* Structural modelling and mutant cycle analysis predict pharmacoresponsiveness of a Na(V)1.7 mutant channel. *Nat Commun* 2012;**3**: 1186.

21. Yang Y, Adi T, Effraim PR. *et al.* Reverse pharmacogenomics: carbamazepine normalizes activation and attenuates thermal hyperexcitability of sensory neurons due to Na(v) 1.7 mutation I234T. *Br J Pharmacol* 2018;**175**:2261–71.

22. Carvill GL, Engel KL, Ramamurthy A. *et al.* Aberrant inclusion of a poison exon causes Dravet syndrome and related SCN1A-associated genetic epilepsies. *Am J Hum Genet* 2018;**103**:1022–9.

23. Voskobiynyk Y, Battu G, Felker SA. *et al.* Aberrant regulation of a poison exon caused by a non-coding variant in a mouse model of Scn1a-associated epileptic encephalopathy. *PLoS Genet* 2021;**17**:e1009195.

24. Solé L, Wagnon JL, Tamkun MM. Functional analysis of three Nav1.6 mutations causing early infantile epileptic encephalopathy. *Biochim Biophys Acta Mol Basis Dis* 2020;**1866**:165959.

25. Drenth JP, Waxman SG. Mutations in sodium-channel gene SCN9A cause a spectrum of human genetic pain disorders. *J Clin Invest* 2007;**117**:3603–9.

26. Arthur L, Keen K, Verriotis M. *et al.* Pediatric erythromelalgia and SCN9A mutations: systematic review and single-center case series. *J Pediatr* 2019;**206**:217–224.e9.

27. McDonnell A, Schulman B, Ali Z. *et al.* Inherited erythromelalgia due to mutations in SCN9A: natural history, clinical phenotype and somatosensory profile. *Brain* 2016;**139**:1052–65.

28. Michiels JJ, te Morsche RH, Jansen JB. *et al.* Autosomal dominant erythermalgia associated with a novel mutation in the voltage-gated sodium channel alpha subunit Nav1.7. *Arch Neurol* 2005;**62**:1587–90.

29. Inserra MC, Israel MR, Caldwell A. *et al.* Multiple sodium channel isoforms mediate the pathological effects of Pacific ciguatoxin-1. *Sci Rep* 2017;**7**:42810.

30. Israel MR, Tanaka BS, Castro J. *et al.* NaV 1.6 regulates excitability of mechanosensitive sensory neurons. *J Physiol* 2019;**597**: 3751–68.

31. Deuis JR, Wingerd JS, Winter Z. *et al.* Analgesic effects of GpTx-1, PF-04856264 and CNV1014802 in a mouse model of NaV1.7-mediated pain. *Toxins (Basel)* 2016;**8**:78.

32. Osteen JD, Herzig V, Gilchrist J. *et al.* Selective spider toxins reveal a role for the Nav1.1 channel in mechanical pain. *Nature* 2016;**534**:494–9.

33. Beckermann TM, McLeod K, Murday V. *et al.* Novel SCN5A mutation in amiodarone-responsive multifocal ventricular ectopy-associated cardiomyopathy. *Heart Rhythm* 2014;**11**:1446–53.

34. Pais LS, Snow H, Weisburd B. *et al.* seqr: a web-based analysis and collaboration tool for rare disease genomics. *Hum Mutat* 2022;**43**: 698–707.

35. Richards S, Aziz N, Bale S. *et al.* Standards and guidelines for the interpretation of sequence variants: a joint consensus recommendation of the American College of Medical Genetics and Genomics and the Association for Molecular Pathology. *Genet Med* 2015;**17**:405–24.